Degradation of bisphenol-A by dielectric barrier discharge system: influence of polyethylene glycol stabilized nano zero valent iron particles

OPEN ACCESS
IOP Publishing
Advances in Natural Sciences: Nanoscience and Nanotechnology
Adv. Nat. Sci.: Nanosci. Nanotechnol. **8** (2017) 035013 (18pp)
https://doi.org/10.1088/2043-6254/aa7714

Degradation of bisphenol-A by dielectric barrier discharge system: influence of polyethylene glycol stabilized nano zero valent iron particles

Jimoh O Tijani[1,2], Massima E S Mouele[1], Ojo O Fatoba[1], Omotola O Babajide[1] and Leslie F Petrik[1]

[1] Department of Chemistry, Environmental and Nano Sciences Research Group, University of the Western Cape, Private Bag X17, Bellville 7535, South Africa
[2] Department of Chemistry, Federal University of Technology, PMB, 65, Bosso Campus, Niger State, Nigeria

E-mail: jimohtijani@futminna.edu.ng

Received 4 January 2017
Accepted for publication 18 May 2017
Published 17 July 2017

Abstract

In this study we report the synthesis and catalytic properties of polyethylene glycol stabilized nano zero valent iron particles (PEG-nZVI) added to the dielectric barrier discharge (DBD) system to induce photo-Fenton process in the degradation of bisphenol A (BPA) in aqueous solution. The influence of operating parameters such as solution pH, initial concentration of the modelled pollutant and PEG-nZVI dosage on the extent of BPA degradation was investigated. The residual concentration of BPA and its intermediates were determined using high performance liquid chromatography (HPLC) and liquid chromatography mass spectrometry (LCMS). The high resolution scanning electron microscope (HRSEM), x-ray diffraction (XRD), Brunauer–Emmett-Teller (BET) surface area, and x-ray photoelectron spectroscopy (XPS) analysis confirmed the formation of filamentous, high surface area iron nanoparticles in the zero valent state. The BPA mineralization rate was monitored using total organic carbon (TOC) analyser. 100% BPA removal was achieved with DBD/PEG-nZVI system within 30 min compared to 67.9% (BPA) with DBD alone after 80 min. The complete BPA removal within a short reaction time was attributed to the existence of a synergetic effect in the combined DBD/PEG-nZVI system. Five new transformation products of BPA namely: 4-nitrophenol ($C_6H_5NO_3$), 4-nitrosophenolate ($C_6H_4NO_2$), 4-(prop-1-en-2-yl) cyclohexa-3,5-diene-1,2-dione, ($C_9H_8O_2$), 4-(2-hydroxylpropan-2-yl)cyclohexane-3,5-diene-1,2-dione ($C_9H_{10}O_3$), and 1,2-dimethyl-4-(2-nitropropan-2-yl)benzene ($C_9H_{10}NO_4$) were identified. BPA degradation proceeded via ozonation, hydroxylation, dimerization, and decarboxylation and nitration step. The combined DBD/photo-Fenton-induced process was found to be the most efficient in the elimination of BPA in aqueous solutions and DBD alone.

Keywords: dielectric barrier discharge system, endocrine disruptors, bisphenol A, nano zero valent iron particles
Classification numbers: 2.03, 4.00

1. Introduction

In the last couple of years increased industrial, high-tech and agricultural activities have enhanced gross domestic products and the standard of living. Conversely, industrial waste such as direct discharge of untreated effluents have contributed to the higher pollution index and hinder the availability of sustainable water supply forcing many citizens to seek and use water from unconventional sources. These negative trends are responsible for the presence and exposure of living organisms to different recalcitrant organic compounds in the environment, which have triggered different health challenges among humans and other species. Some of these chemical-containing products manufactured to meet human needs include: cleansing agents, pharmaceuticals (prescribed and over the counter drugs), polyvinylchloride pipes, cosmetics, fragrances, and toothpaste to mention but a few which are widely used globally. One class of compounds of concern that is currently identified and detected in the global water cycle is endocrine disrupting compounds (EDCs) [1]. Among the EDCs, phenolic compounds such as bisphenol A and its metabolites which are ubiquitous in the water system have become a topical issue because of their endocrine disrupting activities in man and the ecosystem. Bisphenol A (BPA) or 2, 2-bis(4-hydroxyphenyl) propane has been utilized as a monomer or an intermediate in the production of polycarbonate plastics, polyesters, plasticizers, pesticides, thermal printing paper and epoxy resins [2, 3]. BPA enters the receiving waters via discharge of plastic products and household wastewater and is regularly detected in municipal and industrial wastewater at ng l^{-1} to μg l^{-1} concentration [4]. Due to the absence of strong covalent bonds between chemical plastic components and BPA, fragmentation and leaching of BPA from the plastic products under low or high temperature occur [5, 6]. A number of studies have identified drinking water, manufacturing effluents, dust inhalation, agricultural run-off, food and beverage containers as possible exposure routes to this chemical [7]. Exposure to low doses of BPA can cause changes in body weight, cancers, abnormally early puberty, and disorders such as obesity, miscarriage predominantly among fish [8, 9]. BPA also prevents the endocrine hormones such as sex hormones, thyroxin, insulins and leptins from functioning properly and could result in immunotoxic, heptatoxic, carcinogenic and sometimes mutagenic effect [10, 11]. Tay *et al* [6] opined that long term exposure to BPA can cause developmental toxicity, carcinogenicity, neurotoxicity, and estrogenic effect in humans and aquatic species. However, there is lack of reliable data and inconsistency on the neurotoxicity and tetratogenic effects of BPA on animals or humans [10]. Considering the exposure rate to BPA, a precautionary approach vis-a-viz treatment of industrial and municipal wastewater containing BPA prior to discharge into the environment is considered necessary.

However, studies have shown that the degradation of BPA cannot be easily achieved using the current wastewater treatment processes such as coagulation/flocculation, activated carbon adsorption, ultrafiltration, precipitation, biological or chlorination technology due to its lipophilic behaviour, mobility, and non-biodegradability and persistent level [12]. Therefore, it is imperative to develop alternative and sustainable purification techniques to be applied as a polishing step to remove BPA and its fragments from water. This is necessary to safeguard sustainable drinking water as well to protect aquatic organisms against short and long-term health effects. Advanced oxidation technologies (AOTs) have been applied to mineralize organic pollutants into CO_2 and H_2O and other less toxic by-products prior to the discharge into the receiving freshwater by many researchers [13]. Among several AOTs, dielectric barrier discharge (DBD) system has in recent times been considered most effective for the conversion of refractory emerging organic pollutants into inorganic compounds such as carbon dioxide and water. The DBD technology involves the passage of a high-voltage electrical discharge between two electrodes immersed in an aqueous solution to form plasma [14–16]. One of such electrodes is a high voltage electrode, while the other is the ground electrode. The plasma generated can induce both physical and chemical process. The physical process includes strong UV light, local high temperature, and intense shock waves, while the chemical processes are generation of reactive atomic and molecular oxygen-based species such as $OH^{\bullet}$, O_3, $O_2^{\bullet-}$, $HO_2^{\bullet-}$, O, $H^{\bullet}$, H_3O^+ amongst others. In short, these oxygen species together with UV light, and the intense shock wave produced under atmospheric pressure has been widely used for water and wastewater treatment specifically to inactivate microbes and degrade toxic organic pollutants in aqueous solution [17, 18]. The use of the DBD system is considered more advantageous than other AOTs because DBD alone comprises several individual and combined AOTs such as UV-light, H_2O_2, O_3, UV/H_2O_2, UV/O_3, O_3/H_2O_2, or UV/H_2O_2/O_3. On the other hand, when properly designed the DBD system produces ultra violet light and hydrogen peroxide which is not fully maximised within the plasma zone for the mineralization of persistent organic pollutants [18, 19]. In order to properly maximise the UV-light and hydrogen peroxide being produced by the DBD system, the addition of the polyethylene glycol stabilized nano zero valent iron particles to the DBD system was used to induce the photo-Fenton process and enhance the mineralization efficiency of BPA in aqueous solution. However, one problem associated with nano zero valent iron particles is rapid oxidation and aggregation during and after use which reduces the particles' surface area and affects its performance [20]. To overcome these problems, polyethylene glycol was added as stabilizing agent.

Previous studies have shown that the DBD plasma technology can be applied to decompose toxic organic pollutants in wastewater, such as carbamazepine [21], sulfadiazine [22, 23], diclofenac [24], 4-chlorobenzoic acid [25], methylene blue [26], pentoxifylline [17]. However, little or no information exist on the degradation of endocrine disruptor such as BPA using combined DBD system and photo-Fenton induced process. According to the literature survey, it was found that no single advanced oxidation technology on its own is efficient to remove all kinds of contaminants and achieve the desired results, thus the current practice requires a combined approach, which seems to be an attractive option [27]. It is believed that application of combined AOTs will reduce the cost of treatment and increase the mineralization efficiency of the pollutant.

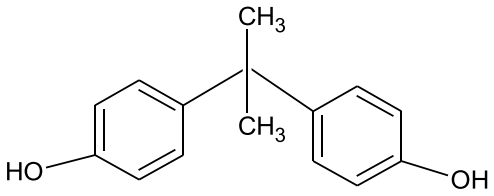

Figure 1. Structure of bisphenol A.

Herein, we investigated the degradation of bisphenol A in aqueous solution using a DBD system followed by induced photo-Fenton process by addition of polyethylene glycol stabilized nano zero valent iron particles (nZVI). To the best of our knowledge, the combination of DBD system and photo-Fenton induced process for the degradation of BPA has not yet been investigated in wastewater treatment. The polyethylene glycol stabilized nZVI synthesised by a modified borohydride reduction method were characterized using high resolution scanning electron microscope (HRSEM), x-ray diffraction (XRD), Brunauer–Emmett–Teller (BET) method and x-ray photoelectron spectroscopy (XPS). The influence of various parameters such as initial pH value, initial concentration of BPA, and dosage of nZVI on BPA degradation efficiency and kinetics rate constant were investigated. In addition, the possible transformation products and degradation pathways were proposed and explained accordingly.

2. Experimental

2.1. Materials

BPA ($C_{15}H_{16}O_2$, 99.5%), iron(III) chloride hexahydrate $FeCl_3.6H_2O$, 50%), polyethylene glycol (99%), sulphuric acid (H_2SO_4, 30%), sodium chloride (NaCl, >99%) were obtained from Sigma Aldrich. While sodium hydroxide solution (NaOH, 98%) and sodium borohydride ($NaBH_4$, 99%), were purchased from Merck. All chemicals were of analytical grade and were used without any further purification. The molecular structure of bisphenol-A is represented in figure 1.

2.2. Synthesis of polyethylene glycol stabilized nano zero valent iron particles

Iron nanoparticles were synthesized via a simple borohydride reduction method. The synthesis involved mixing of 0.75 g $FeCl_3.6H_2O$ dissolved in 20 ml deionized water with 20 ml of 3.5 wt% poly ethylene glycol solution which acted as a dispersing and stabilizing agent. The colour change of the $FeCl_3.6H_2O$ solution from yellow to orange was observed. Thereafter, 0.28 g $NaBH_4$ dissolved in 50 ml deionized water was added drop by drop to the mixture of $FeCl_3.6H_2O$/polyethylene glycol under vigorous stirring until a black precipitate of nZVI was obtained. The reaction was completed and iron nanoparticles were separated using a bar magnet. The synthesised iron nanoparticles were washed with ethanol prior to freeze drying and then labelled PEG-nZVI (JT17). Non-stabilized nZVI was prepared without the addition of 3.5% polyethylene glycol solution to the mixture of $FeCl_3.6H_2O$ and $NaBH_4$.

2.3. Characterization of nano zero valent iron particles

The crystal phases as well as the crystallite size of the prepared PEG-nZVI were determined by powder XRD analysis performed on a Bruker AXS D8 Advance with Cu-Kα radiation. The morphology of the synthesised material was examined using Zeiss Auriga HRSEM. A mass of 0.05 mg synthesised material was sprinkled on carbon adhesive tape and sputter coated with Au–Pd using Quorum T15OT for 5 min prior to analysis. The microscope was operated with electron high tension (EHT) of 5 kV for imaging. A XPS PHI 5400 equipped with hemispherical sector analyser operated using non-monochromated Al-Kα x-rays with energy 1486.6 eV, at 300 W and 15 kV was used to examine the surface elemental composition of the material. The XPSPeak 4.1 software was used for data analysis and peak fits. In the case of BET N_2 adsorption, about 100 mg of the sample was placed in a sample tube, and was first degassed at 90 °C for 4 h to remove residual water and other volatile components that were likely to block the pores. The BET surface area and average pore volume distributions were obtained from the plot of volume adsorbed ($cm^3\ g^{-1}$ STP) versus relative pressure. The N_2 adsorption-desorption isotherms were collected at −196 °C using micromeritics ASAP 2020 accelerated surface area and porosimetry analyser.

2.4. Description of the experimental set-up

Figure 2 represents the schematic diagram of DBD system used for the degradation of the BPA. The device comprised a DBD reactor that generated powerful oxidants such as hydroxyl radicals, hydrogen peroxide, ozone and ultraviolet light, using an AC high voltage power supply, step down transformer, air flow meter, air pump, ground electrode and a reactor vessel containing the model wastewater.

The DBD reactor was a double quartz tube with a quartz inner tube and outer tube diameter of 1 mm and 7 mm, respectively. The AC high voltage power supply was set at 25 V, delivering a current of 5 A and a power of 125 W, and was connected in series to a transformer that steps the AC voltage up to a DC output voltage of ~8 kV. The 0.5 mm silver electrode directly connected to the high voltage (output of the transformer) was immersed in a 50 g l^{-1} of sodium chloride electrolyte placed in the inner quartz tube of the single cell DBD reactor and was also earthed. Air was provided by an air pump with a high and low flow speed switch which was connected to both air flow meter and the single outer quartz cell reactor tube. An air-flow rate of 3.0 l min^{-1} was used through air flow gap. The DBD reactor was 23 cm long with an inlet and outlet for air circulation.

2.4.1. DBD experimental method. The 10 ppm (4.4×10^{-5} M) solution of the prepared BPA was used. 1.5 l of the simulated wastewater was measured and placed in a 2 l beaker. The original depth of the simulated organic wastewater in the reactor vessel was about 130 mm and later rose to about 135 mm due to the flow of air through the DBD which produced bubbles in the solution compartment. The electrical conductivity of the

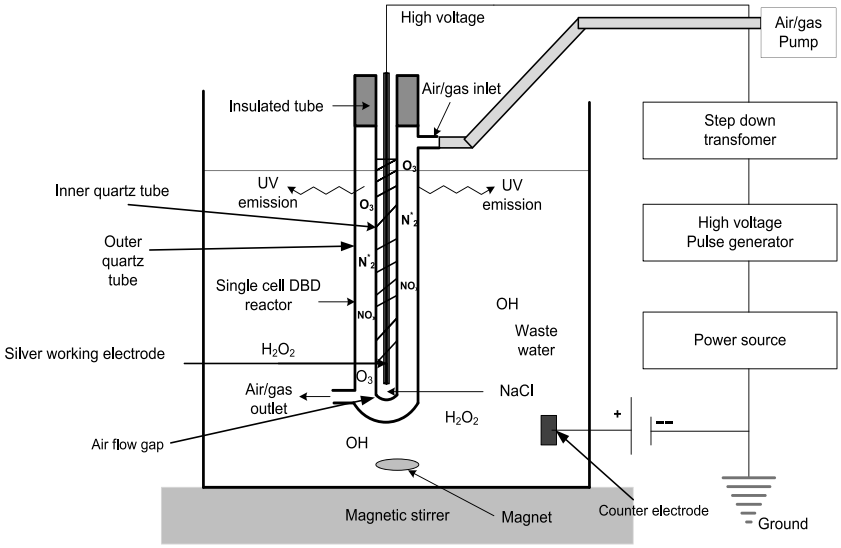

Figure 2. The schematic diagram of the dielectric discharge barrier system.

aqueous solution of BPA was measured to be 20.1 μS cm^{-1} with the aid of multi-parameter analyser C3010. The DBD experiment was conducted for 120 min at room temperature (20 °C) and sampling was done at time intervals of 10 min. The efficiency of the DBD process was determined by measuring the residual concentration of BPA using HPLC. To investigate the influence of pH, the initial solution pH was varied from 3 to 12 for 120 min by adding 0.5 M H_2SO_4 or 0.5 M NaOH dropwise until the desired pH was achieved. The solution pH was measured with a multi-parameter analyser C3010. The initial concentrations of BPA solution were varied in the range of 10–30 ppm maintained at optimum solution pH of 3.

2.4.2. Treatment of BPA by combination of DBD reactor and the stabilized nano zero valent iron (nZVI) particles. The experimental set up remained the same as explained with DBD alone above except that the solution pH was adjusted to 3. 10 ppm of BPA solution was measured into the solution compartment, different amounts of PEG-nZVI (0.02, 0.04, 0.06, 0.08 and 0.1 g) were added corresponding to concentrations of 0.01, 0.03, 0.04, 0.05 and 0.07 g l^{-1} in the solution compartment. Sampling was done from the reactor vessel at time intervals of 10 min and the 2 ml aliquot was filtered with a 0.22 μm membrane filter and analysed using HPLC method described above. The experiment was repeated twice and the average value was reported. The control experiment was carried out in the dark with ordinary PEG-nZVI using different dosage (0.02–0.10 g) at constant conditions of solution pH (3), volume of BPA (1.5 l) and concentration of BPA (10 ppm) while the DBD system was switched off. The mineralization of BPA was monitored in terms of the reduction of total organic carbon (TOC) before and after the oxidation process using standard thermocatalytic digestion followed by non-dispersive infrared (NDIR) detection described by Hu *et al* [27]. The experiments were repeated twice and an average experimental value with a standard deviation below 5% was presented in each case.

2.4.3. Analytical techniques. High performance liquid chromatography (HPLC) (LC-MS 6230, Agilent, USA) equipped with a Waters 1525 binary HPLC pump, Waters 2487 dual λ absorbance detector set at 280 nm and Waters 2707 autosampler running on the Breeze software version 2. A Waters Spherisorb C_{18} reversed-phase liquid chromatography column dimension (150 mm × 4.6 mm × 5 μm) was used for the analysis of BPA concentration. A gradient elution method involving two mobile phases (water:acetonitrile 85:15, (v/v) solution) and the same components with 0:100 (v/v) with a flow rate of 1 ml min^{-1} and injection volume of 20 μl at 26 °C. The Agilent 6230 Time of flight liquid chromatography—mass spectrometry coupled with ultra violet light set at 280 nm in the negative ionization mode was used for qualitative identification of BPA intermediates formed during the decomposition by DBD reactor and DBD/photo-Fenton induced process. The separation of BPA into various fragments was accomplished using a symmetry C8 column (dimension 15 mm × 3.9 mm × 5 μm) and a gradient method containing water (0.1% formic acid), acetonitrile (0.1% formic acid) in the ratio (85:15, 0:100) in 15 min at a flow rate of 0.4 ml min^{-1} and temperature of 20 °C respectively.

3. Results and discussion

3.1. HRSEM analysis of non-stabilised and stabilised nano zero valent iron particles

High resolution scanning electron microscopy (HRSEM) was used to examine the morphology of the prepared nano zero valent iron (nZVI) via the modified borohydride reduction method. The HRSEM images of the prepared non-stabilized nZVI particles (JT16) and polyethylene glycol-stabilised nZVI particles (JT17) of different magnification are depicted in figure 3.

The HRSEM images of sample JT16 at low and high magnification are shown in figures 3(a) and (b). While HRSEM images of sample JT17 at low and high magnifications are

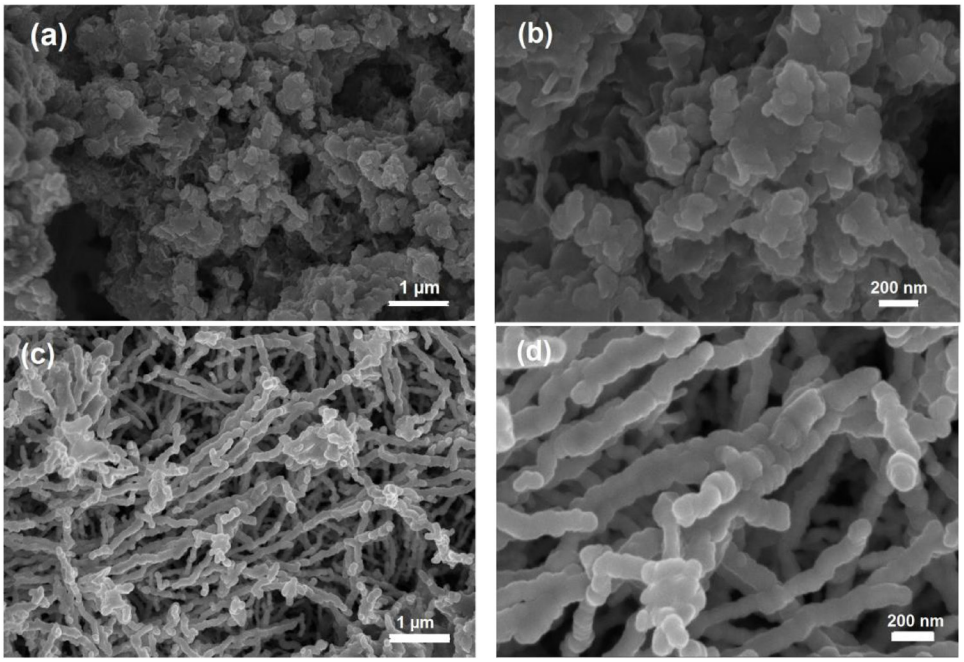

Figure 3. HRSEM micrograph of JT16 (a) at low magnification, (b) high magnification, and of JT17 (c) at low magnification, (d) high magnification.

represented in figures 3(c) and (d). The HRSEM results showed that the JT16 (figure 3(a)) did not resemble a discrete particles but rather appeared in the form of agglomerated and densely packed particles with uneven surface morphologies. In addition, the particles were deposited on one another forming nanoclusters, which are clearly seen in JT16 (figure 3(b)). Thus, the morphology of JT16 at high magnification was irregular. On the other hand, JT17 (figures (c) and (d)) did not produce agglomerated nanoparticles. Instead, the particles are threadlike forming long uniform wires or beads on a string like filament. Thus, the formation of filamentous morphology may be due to the strong intrinsic magnetostatic force of attraction between the Fe nanoparticles. The observed structure in JT17 (figures (c) and (d)) may also be due to the stabilizing effect of polyethylene glycol which prevented the iron nanoparticles from agglomeration into clusters or being oxidised by oxygen in air.

3.2. XRD analysis

The XRD diffractogram of freshly synthesised non-stabilised and PEG-stabilised nZVI is depicted in figure 4.

In figure 4, the broad intense diffraction peak for both JT16 and JT17 at 2θ values of 44.77° which correspond to reflection plane of 1 1 0 (2.01 Å) revealed the formation of iron in the zero valent state, and matched well with JCPDS (00-006-0696). Apart from the broad diffraction peaks observed at 2θ values of 44.77°, there were two additional low intensity diffraction peaks at 2θ value of 65.2° and 82.6° in the PEG-stabilized nZVI which are however absent in the non-stabilized nZVI. These two diffraction peaks corresponded to a reflection plane 2 0 0 (1.43 Å) and 2 1 1 (1.17 Å). Therefore, the presence of the three prominent peaks in the XRD pattern of the PEG-stabilized iron particles at a 2θ value of 44.7°, 65.2° and 82.6° agrees with

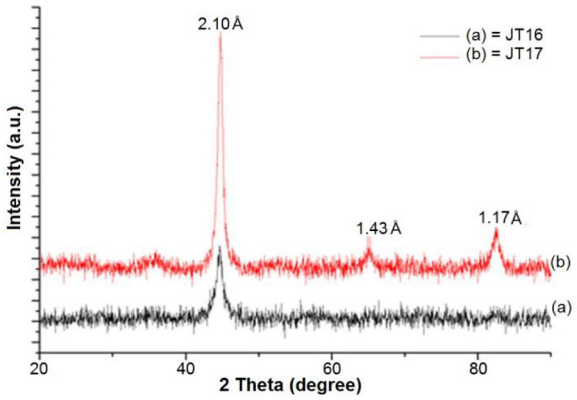

Figure 4. XRD spectrum of sample: (a) JT16 and (b) JT17.

typical nZVI particles. The average particle size was calculated using the Debye Scherer's equation. From the calculation, it was revealed that the particle sizes of non-stabilized and stabilized nZVI were 19.5 nm and 22.6 nm, respectively. The differences in particle size of JT16 (19.5 nm) and JT17 (22.6 nm) could be attributed to the stabilization effect of the polyethylene glycol which prevented rapid particle agglomeration. Furthermore, no other shell or peak corresponding to iron oxide (FeO, Fe_2O_3, Fe_3O_4) were detected. This result corroborates the XPS analysis shown in (figure 5), where metallic Fe in zero state was observed at 707.5 eV in the case of JT17.

3.3. XPS analysis of JT17

Figure 5 represents the full XPS profile of polyethylene glycol stabilized nZVI particles (JT17) and revealed the presence of Fe, C, O and Cu (figure 5(a)). While figures 5(b)–(d) depict the photoelectron measurement of individual elements present in the sample namely: Fe 2p, C 1s and O 1s, respectively.

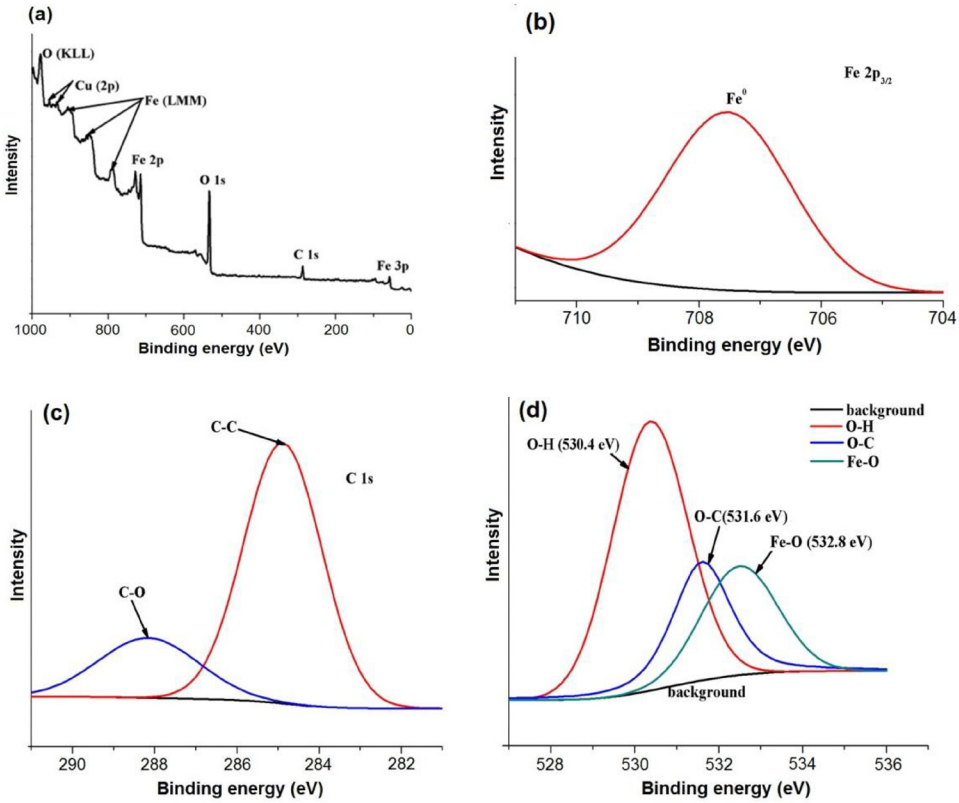

Figure 5. (a) General XPS survey of sample JT17, (b) high resolution XPS profiles of (b) Fe 2p, (c) C 1s and (d) O 1s in JT17.

In figure 5(b), the peak located at 707.5 eV corresponded to Fe $2p_{3/2}$ in the zero valent state. Besides Fe in the nanoparticles, three different carbon peaks were located separately in the binding energy region of 284.8, 286.4 and 288.0 eV shown in figure 5(c), which corresponded to C–C, C=C and C–OH. The carbon signals probably originated from the polyethylene glycol used as a stabilizing agent. The XPS spectrum of the JT17 agreed with the XRD result (see figure 4). Similar observation on the presence of Fe^0 was reported by Xi *et al* [28] on nano zero valent iron particles synthesised from $FeCl_3.6H_2O$ and $NaBH_4$. The Cu shown in figure 5(a) originated from the Cu sample holder. The XPS profile of O 1s shown in figure 5(d) revealed three prominent peaks in the binding energy positions of 530.4, 531.6 and 532.8 eV respectively. The O 1s peak at 530.4 eV corresponded to OH group present in the polyethylene glycol chain while the observed value in the binding energy region of 531.6 eV was assigned to O–C. The O–C suggests bonding of oxygen to carbon which indicates the existence of carbon species from polyethylene glycol in the sample JT17. The observed peak in the binding energy region of 532.8 eV was assigned to O in FeO, which confirmed the existence of Fe oxide particles.

3.4. BET surface area of JT16 and JT17

The surface area and pore size distribution patterns of sample JT16 and JT17 were investigated using micrometrics ASAP 2020 surface area and porosity analyzer. The results of N_2 adsorption-desorption isotherm of JT16 and JT17 as well as pore size distribution are presented in figures 6 and 7.

The BET surface area of JT16 and JT17 as obtained from N_2 adsorption-desorption were 28.82 and 76.77 $m^2\ g^{-1}$, respectively. The BET surface area of JT17 was three times more than JT16, which can be attributed to the use of polyethylene glycol as a stabilizer which prevented aggregation of the individual particles (see HRSEM images shown in figures 3(c) and (d)). According to the International Union of Pure Applied Chemistry (IUPAC) nomenclature, the adsorption isotherms of both samples were type IV isotherms. Sample JT17 exhibited a strong H3 hysteresis loop characteristics of cylindrical shaped pores with wider bodies, which is a characteristic of a mesoporous structure. The mesoporous structure of sample JT17 exhibited a bimodal pore size distribution at relative pressure range of 0.46–1.0. The bimodal pore size distribution was not clearly defined in the case of JT16, which may be as a result of agglomerations of individual particles. The obtained value was far greater than BET surface area of 0.11 $m^2\ g^{-1}$ reported for commercial ZVI [28]. In addition, the pore sizes of JT16 and JT17 were closely related with a narrow distribution range of 1.07–10 nm and 1.22–12.8 nm, respectively. The narrow pore size distribution pattern can be linked to intra-agglomeration among the particles.

3.5. Effect of initial pH on the degradation of bisphenol A

The pH of the solution influences the oxidation of organic compounds in a DBD system and affects the oxidative strength of the reactive species such as H_2O_2, O_3, $^{\bullet}O$ and $OH^{\bullet}$. Based on this background, the influence of variation of solution pH in the range of 3–12 on the degradation of BPA

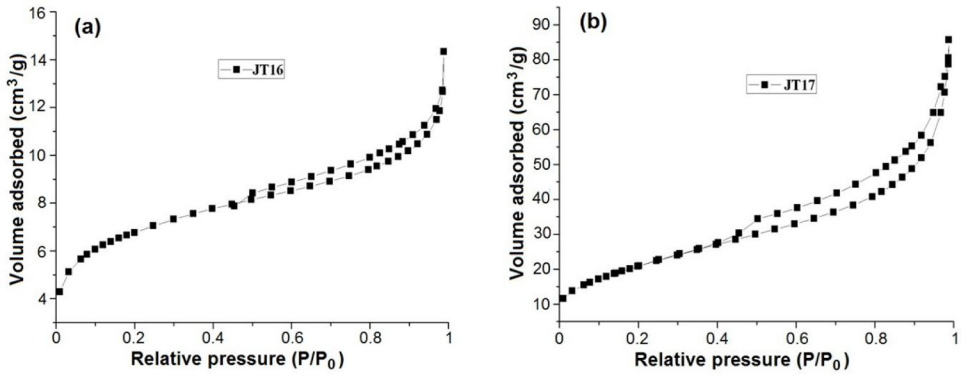

Figure 6. N_2 adsorption-desorption isotherm plot of (a) JT16 and (b) JT17.

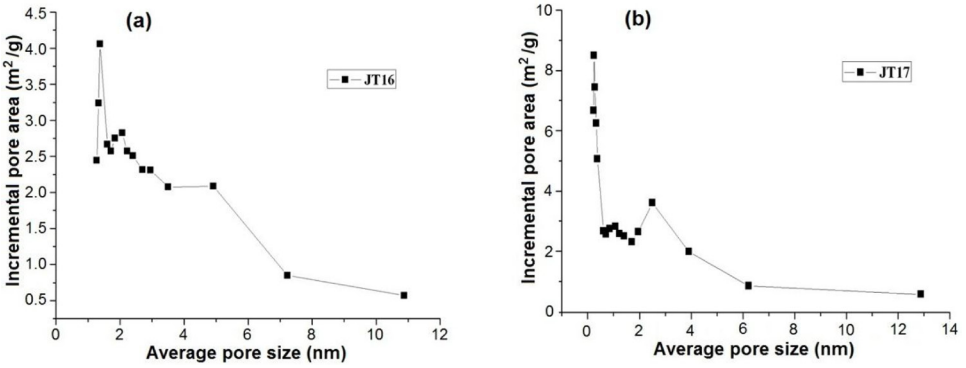

Figure 7. Pore size distribution of (a) JT16 and (b) JT17.

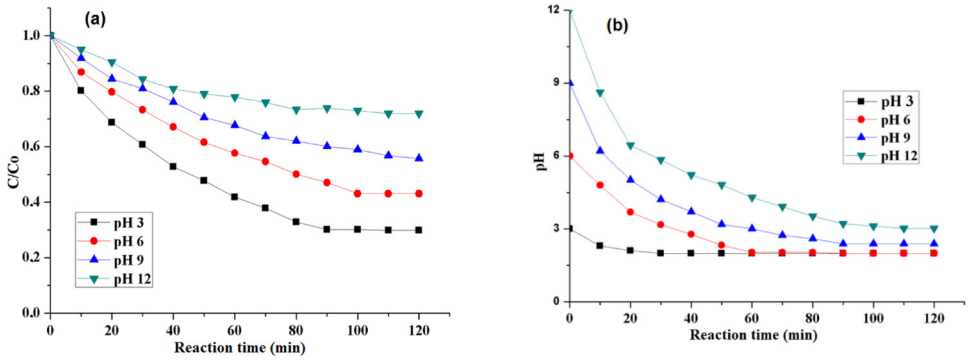

Figure 8. Effect of (a) the initial pH value on the degradation of BPA, and (b) decrease in solution pH values during DBD by discharged voltage 8 kV, volume of BPA is 1.5 l, air flow rate 3 l min^{-1}, electrode is silver, electrolyte NaCl (50 g l^{-1}), concentration of BPA is10 ppm, number of replicates $n = 2$.

by the DBD system was explored. Figure 8(a) shows the effect of pH on the degradation of BPA with time while figure 8(b) represents change in solution pH during the plasma discharge experiment.

As shown in figure 8(a), it can be seen that the removal efficiency of BPA was faster at a lower pH than at a higher pH. The removal efficiency of BPA at pH 3, 6, 9 and 12 was found to be 70.2%, 57%, 45% and 28.1%, respectively, after 120 min. Besides, the removal efficiency of BPA by DBD, the obtained experimental data obtained within 10–80 min at different pH values were fitted to the pseudo-first order kinetic model (plot not shown). It was observed that the apparent reaction rate constant (k) of BPA ($k = 0.0136\,min^{-1}$, $R^2 = 0.9896$) at low pH (pH = 3) reduced to ($k = 0.0038\,min^{-1}$, $R^2 = 0.9589$) at pH 12. This means that acidic conditions favoured the removal and degradation of BPA rather than the alkaline medium. At low pH, O_3 is stable and remains the dominant species and as such was assumed to be responsible for the mineralization of BPA in solution in acidic conditions. Instead, OH^0 radicals with higher oxidation potential in acidic conditions, or perhaps H_2O_2, were responsible for the observed high removal efficiency. This is because a substantial amount of O_3 generated by the DBD escaped from the surface of the solution because the DBD was not a closed system. The open DBD system reduced the concentration of O_3 interacting with the target compounds compared to OH^0. The other possibility may be due to the consumption of oxygen by nitrous (NO) and nitric oxide (NO_2) which consequently reduced the concentration of

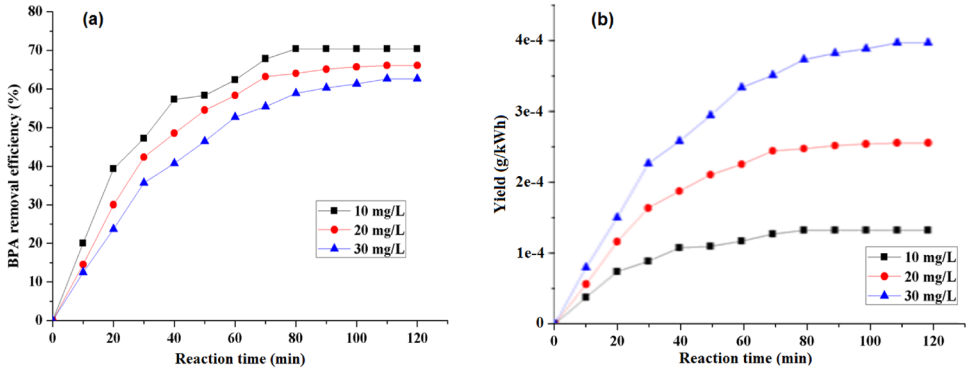

Figure 9. Effect of (a) BPA initial concentration, (b) BPA degradation yield at different concentration values by the DBD system at discharge voltage 8 kV, pH 3, air flow rate 3.0 ml min^{-1}, electrolyte NaCl (50 g l^{-1}), volume of BPA is 1.5 l, electrode is silver, number of replicates is 2.

O_3 in the system. At a higher pH (basic region), the formation of OH^0 was expected to predominate and accelerate the oxidation of BPA molecules. On the other hand, lower removal efficiency of BPA was observed. The most possible reason for low removal efficiency under strongly alkaline conditions (high pH) could perhaps be linked to the generation of CO_2 during the oxidation of BPA, which perhaps formed carbonate ions (CO_3^{2-}) and HCO_3^-. These carbonate species (CO_3^{2-} and HCO_3^-) are known as radical scavengers and consume OH radicals owing to their high rate constant value. The decrease in the amount of OH radicals in solution would then have affected the removal efficiency. The outcome of this study is however contrary to the findings reported by [6, 28] on BPA oxidation via ozonation process. The two authors found that BPA degradation rate increased with the increase in solution pH from 2 to 12. The reason for the inconsistency in the result reported by the two authors and the outcome of this study was that, a radical scavenger (t-BuOH) was added by those authors to scavenge and consume available OH^0. This action eliminated the stronger competition between OH^0 and O_3 for the organic pollutants. Thus, it was demonstrated that only O_3 reacted with BPA. Whereas in this study, radical scavengers were not added to the DBD system to consume OH, thus creating room for stronger competition among O_3, OH^0 and H_2O_2 for the organic pollutants.

Figure 8(b) represents variation in solution pH monitored during the oxidation process. It was found that the initial pH values reduced significantly on exposure to plasma discharge especially at higher pH values as the reaction time increases. The decrease in the solution pH upon exposure to plasma generated via dry air may be due to the formation of carboxylic and mineral acids. Furthermore, the release of phenolic fragments by bisphenol A during the oxidation process may also contribute to the solution acidity and low pH. The presence of OH^0 in the solution may also have accelerated the formation of NO and NO_2 to HNO_2 and HNO_3 respectively, thus contributed to the solution acidity index value. A similar decrease in solution pH of sulfadiazine or carbamazepine was reported by [20] upon exposure to plasma and [22]. Based on the experimental data, the optimal degradation pH for BPA was found to be 3.0, thus subsequent experiments were carried out at this pH value.

3.6. Effect of initial concentration of BPA

The influence of different initial concentration of BPA on the degradation efficiency and yield in the range of 10–30 mg l^{-1} under the optimal conditions of pH 3, discharge voltage 8 kV, air flow rate 3 ml min^{-1} were investigated. The removal efficiency and degradation yield of BPA as a function of reaction time is shown in figures 9(a) and (b).

As shown in figure 9(a), the BPA removal efficiency after 80 min reaction time at 10 mg l^{-1} concentration and at pH 3 and discharge voltage 8 kV was 70.4%, and however reduced to 58.9% as the BPA concentration was increased to 30 mg l^{-1}. As expected, the removal efficiency of BPA was greater at lower concentration than at higher concentrations. This could be attributed to the relative number of BPA molecules competing with the few DBD generated reactive species during the plasma discharge. On the other hand, at higher pollutant concentration, the number of BPA molecules at the fixed conditions applied increased without a corresponding increase in the concentration of the DBD generated free reactive species. As a result, the concentration of available oxidant species was lower and could not effectively mineralize large numbers of BPA molecules into harmless compounds. This resulted in lower removal efficiency as seen at higher concentration of the pollutants. The other possibility for lower removal efficiency could be due to the formation of refractory secondary transformation products at higher pollutant concentrations, which probably competed with the original BPA compound for free reactive species. The competition between the intermediates and initial compound may have prevented further degradation of the original compound and thus have caused the lower degradation efficiency. This observation is in agreement with previous studies reported by researchers on endocrine disruptors in spite of the differences the DBD configurations [19, 23, 29].

Furthermore, the degradation efficiency of BPA was explained in terms of degradation yield (Y) as shown in figure 9(b), which represents the rate of oxidation of the pollutants per unit energy consumed during the process as expressed in following equation

$$Y = \frac{CVX}{100Pt}, \tag{1}$$

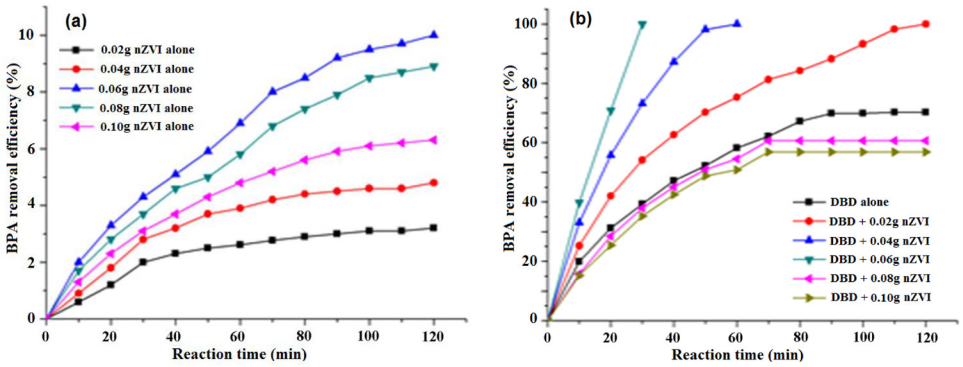

Figure 10. Removal efficiency of (a) BPA by different dosage of stabilized nZVI alone (JT17), (b) BPA by DBD combined with different dosages of nano zero valent iron (experimental conditions: BPA volume 1.5 l; BPA concentration 10 mg l^{-1}; discharged voltage 8 kV; air flow rate 3 ml min^{-1}; solution pH 3; NaCl electrolyte concentration 50 g l^{-1}; electrode (silver), number of replicates = 2.

where C(g l^{-1}) represents initial concentration of the pollutants, V(l) is the volume of the aqueous solution, P(kW) is the average power dissipated, which is expressed as the product of the discharge voltage (V) and applied current (A), t(hour) is the treatment time, while the conversion X(%) is the same as removal efficiency at each treatment time [17]. Contrary to the trend observed in figure 9(a), the degradation yield of BPA increased with increasing pollutant concentrations. According to figure 9(b), the degradation yield of 10 mg l^{-1} BPA solution after 80 min treatment time was 1.32×10^{-4} g kW^{-1} h^{-1}, which however increased to 3.73×10^{-4} g kW^{-1} h^{-1} as concentration increased to 30 mg l^{-1}. The degradation yield of 30 mg l^{-1} solution of BPA was 3 and 1.55 times greater than that obtained with 10 mg l^{-1} and 20 mg l^{-1} solution of BPA under the applied experimental conditions. It is obvious that the increase in the degradation yield at higher pollutant concentration did not depend on the amount of free reactive species in the DBD but on the number of molecules taking part in the reactions. It was found that increases in the concentration of BPA resulted in the corresponding increase in the discharge energy and hence the degradation yield. This observation supported previous investigation reported for different organic pollutants: 17β-estradiol [19], 4-chlorobenzoic acid [25], pentoxifylline [17]. Thus, considering the fact that the removal efficiency was faster and consumed less energy at a lower concentration, 10 mg l^{-1} was selected as the optimal initial concentration for both compounds in this study.

3.7. Degradation of BPA by combined DBD and photo-Fenton induced process

The DBD reactor produces H_2O_2 and intense ultraviolet light which are not maximally utilized. Thus, in order to induce photo-Fenton process and enhance the degradation rate of BPA or 2-NP, different dosage of polyethylene glycol nano zero valent iron (nZVI) particles in the range of 0.02–0.1 g was added to the DBD reactor. The BPA removal efficiency with respect to different dosage of nZVI added to the DBD reactor with the reaction time is illustrated in figure 10.

Figure 10(a) shows the control experiment conducted using different doses of nZVI sample (JT17) alone without the DBD system at the optimum solution pH of 3. It can be observed from figure 10(a) that the removal efficiency of BPA using nZVI sample JT17 alone was in the range of 5–10% after 2 h. This slight percentage decrease of BPA in aqueous solution was attributed to the adsorption phenomenon of the catalyst, which can be ignored when compared to the removal efficiency obtained either by DBD alone or combined DBD/nZVI. Also from figure 10(b), it was found that BPA degradation efficiency at 30 min via DBD system alone was 39.3% and the value increased till 60 min. Beyond 60 min, there was no further increase in the removal efficiency of BPA, which can be ascribed to the resistance of transformation products formed via the degradation process.

With the addition of 0.02 g nZVI, the pollutants degradation efficiency was rapid, reaching 57.1% at 30 min reaction time. When 0.04 g nZVI (JT17) was added to the DBD reactor, the removal efficiency of BPA at 30 min was 73%. With the addition of 0.06 g nZVI to the DBD system containing BPA, 100% or complete removal of BPA were achieved at 30 min. The increase in removal efficiency during the initial stages of combined DBD and photo-Fenton induced reaction compared to DBD alone may probably be attributed to the presence of UV/H_2O_2 in solution which probably facilitated the photoreduction of hydroxylated ferric ion (Fe-OOH^{2+}) leading to formation of ferrous ion (Fe^{2+}) and OH^0 radicals according following equations [30]

$$Fe^{2+} + H_2O_2/UV \rightarrow Fe^{3+} + OH^0 + OH^-, \quad (2)$$

$$Fe^{3+} + H_2O_2 \rightarrow Fe - OOH^{2+} + H^+, \quad (3)$$

$$Fe - OOH^{2+} + UV \rightarrow Fe^{2+} + OH^0. \quad (4)$$

Additionally, the rapid oxidation reaction of Fe^0 to Fe^{2+} and subsequent reaction of Fe^{2+} with UV/H_2O_2 produced more OH radicals

$$Fe^0 + H_2O_2/UV \rightarrow Fe^{2+} + 2OH^0. \quad (5)$$

The two additional sources of OH^0 may perhaps be responsible for such initial higher removal efficiency and complete elimination observed at a short reaction time of 30 min. Therefore, nZVI exhibited the best catalytic activity at a dosage of 0.06 g. The possible explanation for this trend could be that with the addition of 0.02 and 0.04 g nZVI, the amount of Fe^{2+} in

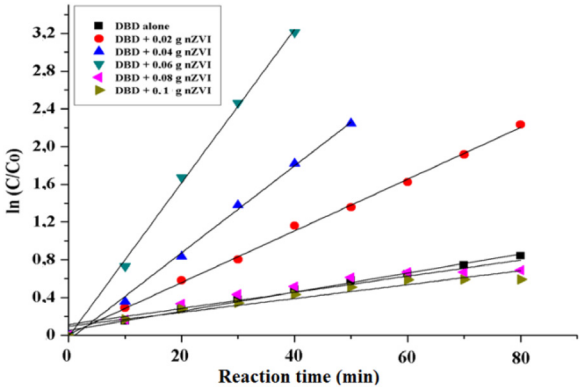

Figure 11. Pseudo-first-order plots for the degradation of BPA by combination of DBD with different dosage of nZVI (JT17). The experimental conditions are the same as in figure 10.

Table 1. The pseudo-first rate constant and correlation coefficient value for BPA degradation via combined DBD/photo-Fenton induced process.

Pollutants	Treatment process	Rate constant (min^{-1})	Correlation coefficient (R^2)
BPA	DBD alone	0.0103	0.9921
	DBD + 0.02 g nZVI	0.0274	0.9984
	DBD + 0.04 g nZVI	0.0462	0.9974
	DBD + 0.06 g nZVI	0.0815	0.9999
	DBD + 0.08 g nZVI	0.0075	0.9335
	DBD + 0.1 g nZVI	0.0073	0.9227

Experimental conditions: BPA volume 1.5 l; BPA concentration 10 mg l^{-1}; discharged voltage 8 kV; air flow rate 3 ml min^{-1}; solution pH 3; NaCl electrolyte concentration 50 g l^{-1}; electrode (silver), number of replicates = 2.

solution required to react with UV/H_2O_2 to induce the photo-Fenton reaction and liberate OH^0 was small. The low yield of OH^0 in the solution may be responsible for the lower removal efficiency compared to 0.06 g nZVI. Thus, with the addition of 0.06 g nZVI to the DBD reactor, it is believe that more of Fe^{2+} was able to react with UV/H_2O_2 to produce OH radicals and Fe^{3+} (equation (2)).

Conversely, with the addition of 0.08 g and 0.1 g, the BPA degradation efficiency decreased abruptly. In fact, the removal efficiency in both cases was lower than the removal rate obtained with alone DBD alone. This may be due to the fact that, the higher nZVI dosage beyond 0.06 g, made the solution highly turbid. The high level of turbidity impeded the UV-light intensity and penetration path leading to light scattering and thus pollutants were not decomposed by free radicals. In addition to the shielding effect which affects UV light penetration, the reaction between Fe^{2+} and H_2O_2/UV that leads to the formation of OH^0 was affected. Thus, the low concentration of OH^0 may also be responsible for lower removal efficiency of BPA. Goi and Trapido [31] and Trapido *et al* [32] submitted that the effectiveness or performance of a photo-Fenton process regarding decomposition of refractory organic pollutants depends on the dosage of Fe^{2+} invariably Fe^0. The authors affirmed that the photo-Fenton process would be less effective in a solution containing excess Fe^{2+}.

3.8. The kinetic model for BPA oxidation

In order to further demonstrate the effectiveness of the combined DBD/photo-Fenton induced process over DBD alone on the removal efficiency of BPA, the obtained experimental data shown in figure 11 were fitted to the pseudo-first order kinetic model in following equation

$$\ln\frac{C_p}{C_{p_0}} = -kt, \tag{6}$$

where t represents the reaction time (min), C_{p_0}connotes initial at time $t = 0$, while C_p is the concentration at a given time t. The pseudo-first order kinetic plot of experimental data obtained via the degradation of BPA by DBD/photo-Fenton induced reaction is shown in figure 11. The experimental data obtained up to 80 min reaction time were used for the kinetic plots since no significant improvement in the BPA degradation efficiency was noticed after this time. The slopes of the individual fitted straight line corresponds to the reaction rate constant k. Furthermore, the rate constant and correlation coefficient of the DBD/photo-Fenton induced process degradation of BPA was determined and represented in table 1.

According to table 1, it is apparent that addition of different doses of nZVI in the range of 0.02–0.06 g DBD system enhanced the degradation rate constant from 0.0274 min^{-1} to 0.0815 min^{-1} for BPA. The degradation reaction rate constant of BPA was eight times greater with the addition of 0.06 g nZVI to the DBD system than with the DBD alone. The experimental data could be better described using pseudo-first order kinetics as evident in the correlation coefficient (R^2) value that was closed to unity. This showed that the addition of nZVI at an optimum dose increased the concentration of hydroxyl radicals in the solution, which in turn enhanced the degradation efficiency of the BPA. On the contrary, further addition of nZVI dosage beyond 0.06 g resulted in the reduction of the reaction rate constant. A slight deviation from pseudo-first plot was observed with the increase in dosage of nZVI from 0.08 to 0.1 g as revealed by the correlation coefficient value (R^2). This showed that beyond the optimal value of 0.06 g, other obtained experimental data precisely from 0.08 g to 0.1 g dosage poorly fitted the pseudo-first order kinetics. This supports that further addition of nZVI to DBD increased the wastewater turbidity level, and inhibited the UV-light intensity. Aside from that, the formation of free reactive species was limited and the interaction between the pollutants and oxidants affected, thus also responsible for such lower rate constant. Very recently [23] found that higher concentration of Fe^{2+} in solution did not translate to higher pollutant mineralization rate due to stronger competition between organic pollutants and excess Fe^{2+} in the solution for free radicals such as OH radicals.

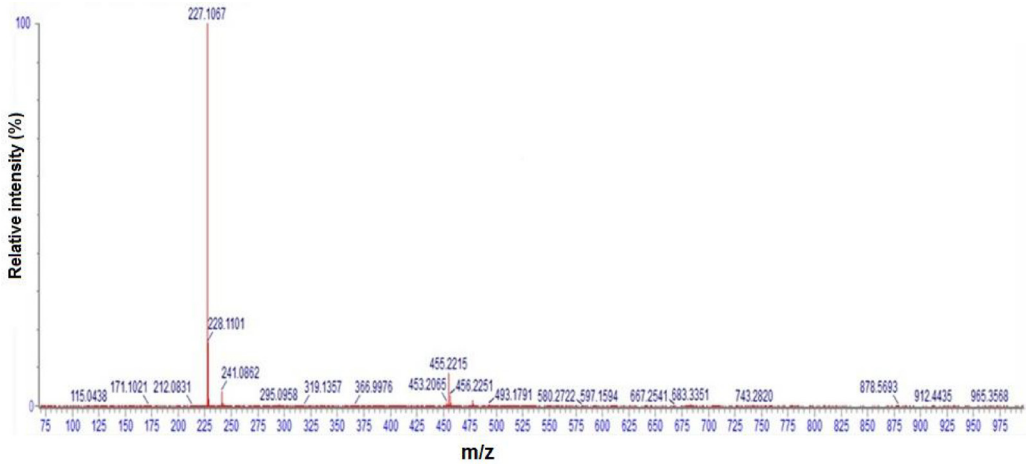

Figure 12. LC-MS spectrum of standard BPA solution prior to oxidation process either by DBD alone or DBD/photo-Fenton induced process.

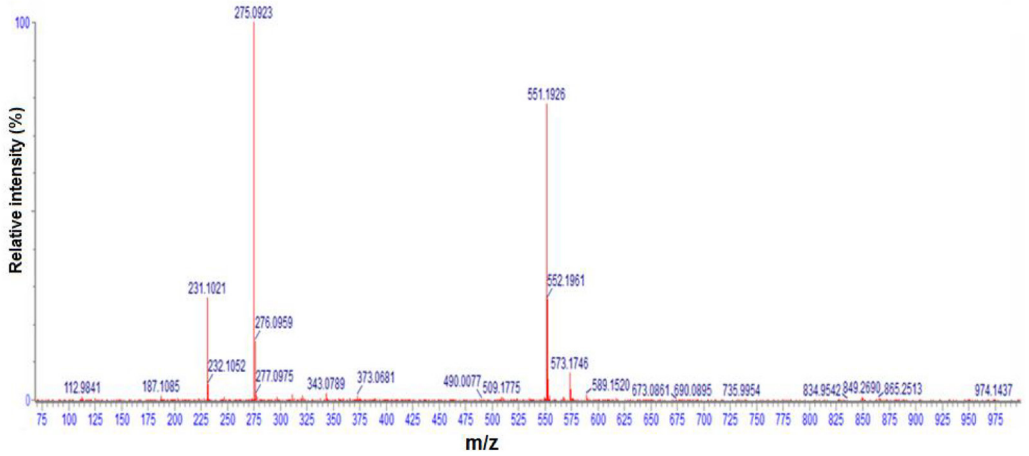

Figure 13. LC-MS spectrum of the intermediates products formed via DBD alone within 20 min reaction time.

3.9. Identification of transformation compounds

The agilent 6230 time of flight liquid chromatograph mass spectrometer (TOF LC-MS) in the negative ionization mode was used for qualitative identification of the intermediates at every 20 min for 2 h. The intermediate compounds formed during the degradation of BPA via DBD and DBD/photo-Fenton induced process is explained as follows.

3.9.1. BPA and BPA oxidation by-product. Figure 12 illustrates the mass spectra (MS) of BPA standard solution or starting material measured in the electrospray ionization (ESI) negative mode, which contained a sharp peak of deprotonated molecular ion $[M\text{-}1]^-$, *m*/*z* at 227.10 within 6.5 min. This means that the original mass of BPA was 228.29 but was measured to be 227.10.

After the exposure of BPA to plasma discharge or radical environment (using either DBD alone or combined DBD/photo-Fenton induced process) several other prominent peaks of different relative molecular masses (*m*/*z*) were noticed in the aliquot with retention time in the range of 1.9 min–5.8 min as shown in figure 13.

Within the first 20 min using DBD alone, BPA oxidised to five by-products with main fragment (*m*/*z*) value of 275.09, 231.10, 187.10 and 551.19 and 112.98. However, the intermediates with mass fragment ion at *m*/*z* 112.98 could not be detected by MS possibly due to low concentration. The LC-MS of the four intermediates are shown in figure 13. The mass difference between 275.09 and fragment ion at *m*/*z* 231.10 was 44, which corresponded to the losses of CO_2. While the mass differences between 275.09 and 187.10 was 88, which indicated two consecutive loss of CO_2. The fourth intermediate compound with a higher molecular weight having a fragmentation pattern (*m*/*z*) at 551.19 was suspected to be a dimeric or an oligomeric compound. This was a result of secondary reactions between two molecules of 275.09. Based on the obtained fragmentation patterns as demonstrated in the MS spectra and available MS library, the following chemical structure were predicted for BP1, BP2, BP3 and BP4: 275.09 ($C_{15}H_{16}O_5$), 231.10 ($C_{14}H_{16}O_3$), 187.10 ($C_{13}H_{16}OH$) and 551.19 ($C_{30}H_{30}O_{10}$), respectively, using BPA ($C_{15}H_{16}O_2$) as a starting compound. Furthermore, there was no difference in the range of intermediate compounds formed after 40 min using DBD alone (MS spectra not shown), which showed that the compounds were stable and resistant.

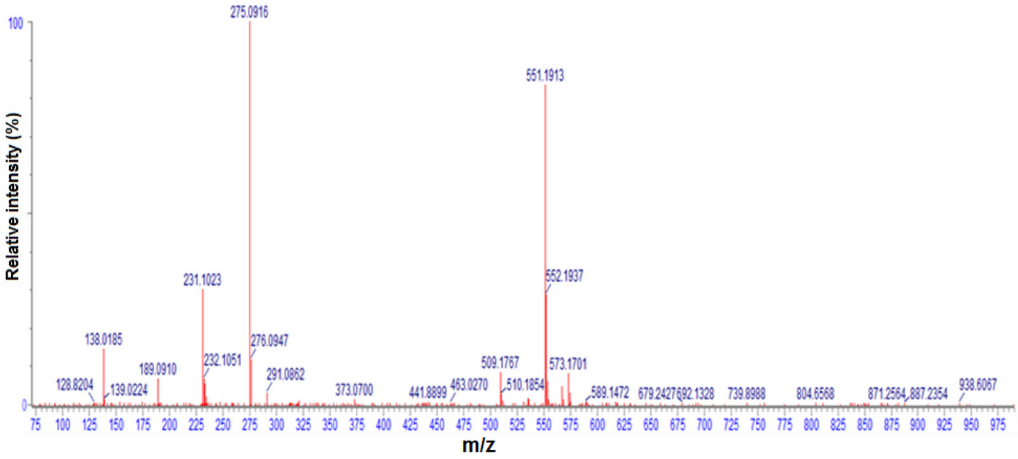

Figure 14. LC-MS spectrum of the intermediates products formed via DBD alone at 60 min reaction time.

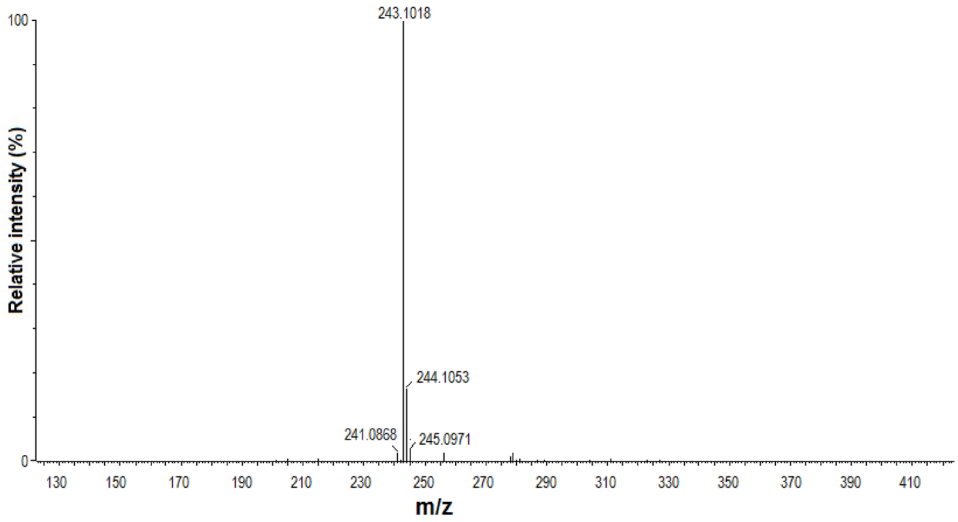

Figure 15. LC-MS spectrum of the intermediates products formed via DBD/photo-Fenton induced reaction (JT17) within 20 min reaction time.

With DBD alone, at 60 min, a new by-product (BP5) with mass fragment ion at *m*/*z* 138.01 was observed with other intermediates still in solution (figure 14).

The observed fragmentation pattern at *m*/*z* 138.01 indicated cleavage of C-C bond of one of the two aromatic rings in BPA molecules into smaller moieties. The cleavage of one of the two aromatic rings suggested hydrogen abstraction from the methyl group (CH_3) by OH radicals. It should be noted that electron-donating species such as OH^0 increase the electron-density of the aromatic rings and made the double bonds more susceptible to subsequent attacks. Based on the available MS library database, the chemical formula of BP5 with fragment ion at *m*/*z* 138.01 was predicted to be $C_6H_5NO_3$ (4-nitrophenol). It had earlier been pointed out that DBD produces nitrogenous species such as nitrous and nitrite oxide, which emanated from the feed dry air. The formation of a nitrogeneous species suggested reaction of phenolic moieties with NOx in the solution. It should be mentioned that similar intermediate compounds observed in solution at 60 min were still the same as those found at 120 min. This suggested that the intermediates were persistent or resistant to further oxidation by the reactive species.

3.9.2. Intermediates compound obtained via DBD/photo-Fenton induced process. On the other hand, when the combined DBD/photo-Fenton induced process was applied to decompose BPA, unlike what was obtained with DBD, only one intermediate compound was formed within the first 20 min. The obtained intermediate compound (BP6) with fragmentation pattern at (*m*/*z*) 243.10 is shown in figure 15. Comparing compound BP6 with the parent compound BPA ($C_{15}H_{16}O_2$), it was found that the compound (BP6) has one additional oxygen which corresponds to an OH^0. Based on this, the chemical structure of BP6 is proposed to be $C_{15}H_{16}O_3$ (mono-hydroxylbisphenol A).

At 40 min, the MS spectra revealed only one peak (not shown), with mass fragment pattern at *m*/*z* 241.89. This corresponded to the loss of hydrogen molecules due to oxidation when compared to 243.10. According to the fragmentation patterns, $C_{15}H_{14}O_3$ is proposed as the chemical formula of the BP7. At 60 min, three different deprotonated molecular ions were observed on the MS spectra at *m*/*z* value of 275.09, 231.10, and 138.01 as shown in figure 16. This corresponds to BP1, BP2 and BP5 which had been previously observed with DBD alone.

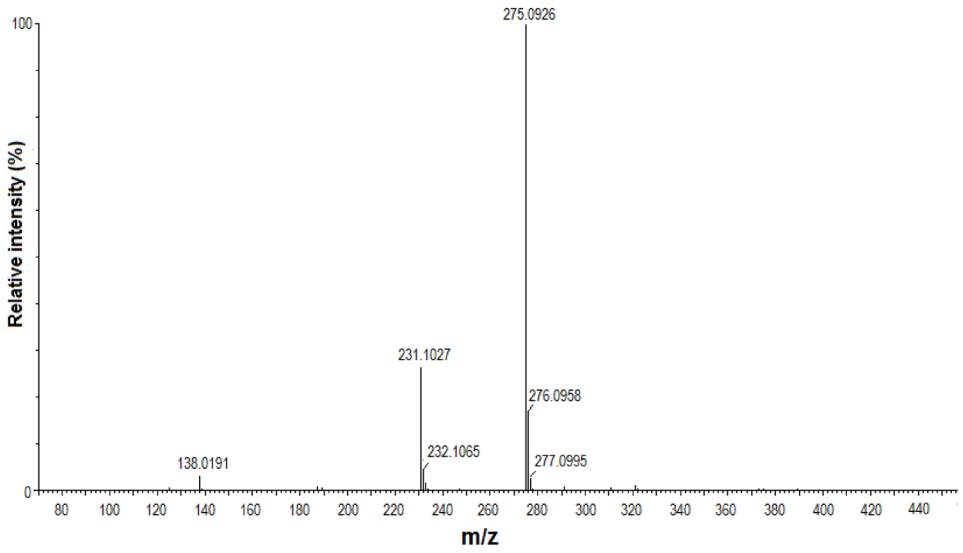

Figure 16. LC-MS spectrum of the intermediates products formed via DBD/photo-Fenton induced reaction at 40 min reaction time.

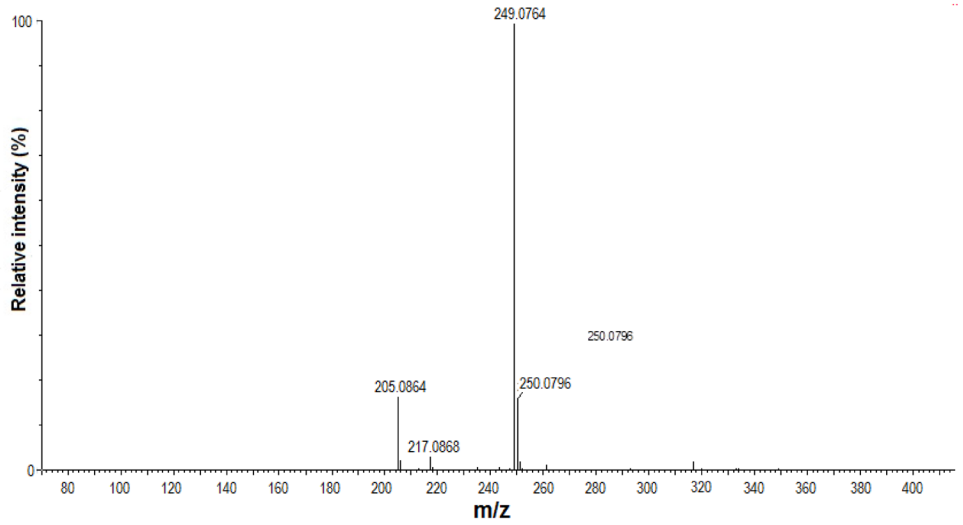

Figure 17. LC-MS spectrum of the products formed via DBD/photo-Fenton induced reaction (JT17) within 80 min reaction time.

At 80 min, three fragmentation patterns at *m/z* 249.07, 217.06 and 205.08 for compounds BP8, BP9 and BP10 were found on the MS spectrum in figure 17.

The fragmentation pattern at *m/z* 249.07 corresponded to loss of the carbonyl group (CO) by a compound with *m/z* value of 275.09. While the elimination of carbon dioxide (CO_2) by an intermediate with fragmentation pattern at *m/z* 249.07 produced compound BP10 with *m/z* at 205.08. As regards the fragmentation patterns at *m/z* 217.06, the difference between this fragmentation pattern and 249.07 was 32, which corresponded to the loss of oxygen molecules. The following chemical formulas are proposed for BP8 ($C_{13}H_{14}O_5$), BP9 ($C_{13}H_{13}O_3$) and BP10 ($C_{12}H_{14}O_3$). At 120 min, with combined DBD/photo-Fenton induced reaction as shown in figure 18, three prominent deprotonated molecular ions appeared at *m/z* 241.89, 196.6 and 146.96. However, the molecular formula of fragment ion at 103.92 could not be identified by the LC-MS instrument probably because it was below detectable limits. The presence of low molecular weight compounds at 120 min for the combined system suggests the cleavage of the two aromatic rings into smaller moieties. According to the MS library, the following molecular formulas are proposed: 195.9 ($C_9H_{11}NO_4$) and 146.9 ($C_9H_8O_2$)

Furthermore, the obtained transformation products during the oxidation of BPA via two degradation systems namely: DBD alone and DBD/photo-Fenton induced reaction are illustrated in the time based scheme in figure 19. As demonstrated in the time scheme experiment shown in figure 19, it is evident that the transformation products obtained via the two degradation systems were different. The differences in the number of intermediates also demonstrated that BPA followed different degradation routes or pathways depending on the process applied. It should be noted that a higher number of intermediates were obtained via DBD alone, which suggests a high level of persistency or stability of intermediates and can be ascribed to the low concentration of free reactive species generated in the DBD system. On the contrary, similar and fewer intermediate compounds were detected in the combined DBD/photo-Fenton induced process (JT17) except at 120 min. The low number of intermediates in the combined system

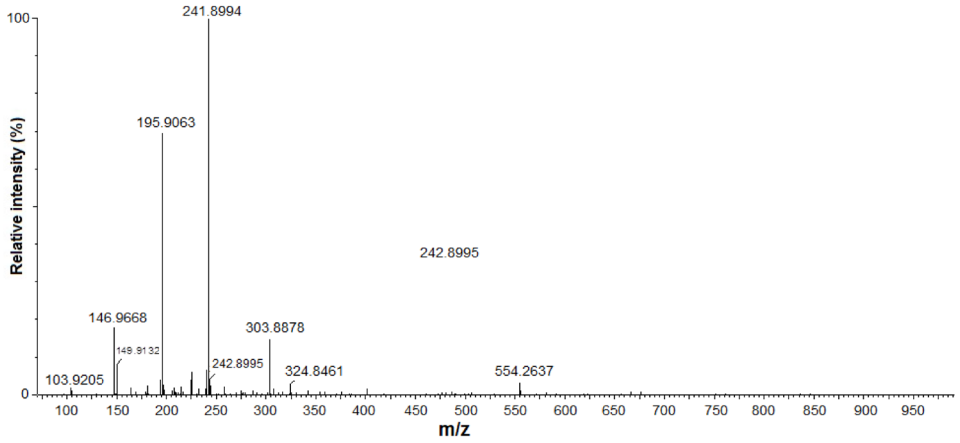

Figure 18. LC-MS spectrum of the intermediates products formed using DBD/photo-Fenton induced process within 120 min reaction time.

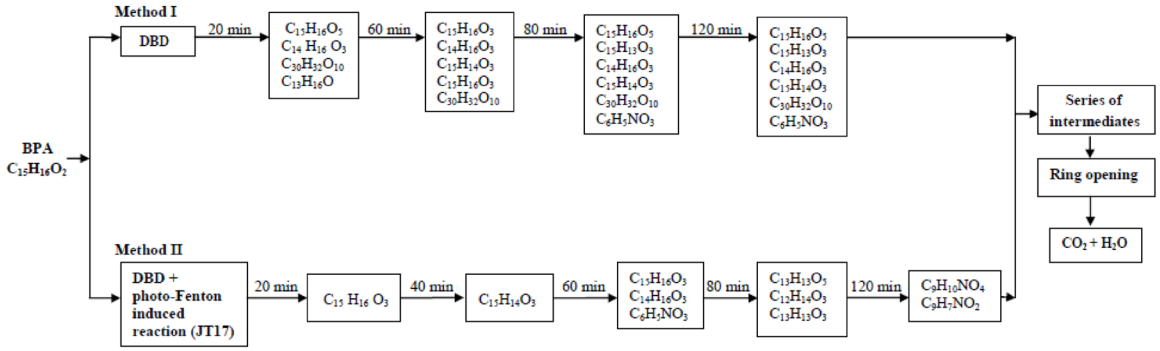

Figure 19. Time based identification of BPA intermediates via DBD alone and DBD/photo-Fenton induced reaction.

compared to DBD alone suggested fast reaction kinetics between the BPA and the reactive species. This also suggested higher concentrations of the reactive species in the combined systems than in DBD alone, which were responsible for the formation of low molecular weight intermediates and further indicated the existence of synergetic effects.

All the intermediate compounds formed via the two processes are summarised with their proposed chemical structure in table 2. The chemical structures are proposed using the MS library.

3.10. Proposed degradation pathways for the obtained oxidation products from BPA degradation via DBD and DBD/photo-Fenton induced reactions

Based on the obtained intermediates shown in table 2, a route for the degradation of BPA to BP4 was proposed and illustrated in the figure 20.

3.10.1. Formation of BP1–BP4. The degradation mechanism of BPA which resulted in the formation of BP1–BP4 within 20 min is shown in figure 20. As earlier shown in table 2, the number of oxygens increased to 5 when compared to the starting compound with two oxygens, which means three oxygens were added, thus suggests that the step I in the oxidation of BPA by DBD was ozonation by an electrophilic substitution reaction. This indicates that BP1 ($C_{15}H_{16}O_5$) was formed by direct electrophilic substitution reaction of ozone with BPA to give an ozonide derivative. The ozonide derivative further undergoes intramolecular rearrangement to yield BP1. Step II involved the loss of CO_2 by BP1 ($C_{15}H_{16}O_5$) to give BP2 ($C_{14}H_{16}O_3$), which otherwise is known as a decarboxylation reaction. The third oxidation by-product (BP3) was obtained directly via a double decarboxylation reaction on BP1 ($C_{15}H_{16}O_5$) (Step III). BP4 was a product of the dimerization reaction involving two similar intermediate compounds. Since the *m/z* was 551.19 ($C_{30}H_{32}O_{10}$), it was possible to conclude that the step IV (figure 20(b)) was addition of two $C_{15}H_{16}O_5$. The proposed mechanism has demonstrated that oxidation of BPA proceeds via ozonation, decarboxylation, double decarboxylation and dimerization reaction to produce recalcitrant intermediate compounds BP1–BP4. The formation of BP1–BP3 via ozonation and photocatalytic process has previously been reported in the literature with exception of BP4 [6, 33].

3.10.2. Formation of BP5–BP7. Furthermore, the proposed degradation pathways for compounds BP5–BP7 is shown in figure 21, it is obvious that compound BP6 ($C_{15}H_{16}O_3$) was formed via two degradation routes: via a hydroxylation step or direct electrophilic substitution of ozone on the aromatic rings of BPA. This indicated that the two reactive species produced by the DBD were probably responsible for the formation of BP6. This corroborates previous studies where it was demonstrated that the mechanistic formation of BP6 proceeds through both hydroxylation and ozonation reactions [6]. The similar intermediate compound during the

Table 2. Transformation products of BPA via the three treatment methods.

Compounds	Molecular formula	Molecular mass (g mol^{-1})	Theoretical mass (*M–H*)	Observed fragment ion at *m/z* value (% abundance)	Acquisition or retention time
Bisphenol A	$C_{15}H_{16}O_2$	228.29	228.26	227.107 (100)	6.5
BP1	$C_{15}H_{16}O_5$	276. 28	276.24	275.09 (97.50)	4.8
BP2	$C_{14}H_{16}O_3$	232.28	232.24	231.10 (97.50)	4.6
BP3	$C_{30}H_{32}O_{10}$	552.55	552.46	551.19 (97.50)	9.9
BP4	$C_{13}H_{16}O$	188.23	188.26	187.10 (84.5)	4.5
BP5	$C_6H_5NO_3$	139.10	139.09	138.01 (45.62)	4.4
BP6	$C_{15}H_{16}O_3$	244.28	244.25	243.10 (97.57)	5.8
BP7	$C_{15}H_{14}O_3$	242.27	242.23	241.89 (66.5)	5.0
BP8	$C_{13}H_{14}O_5$	250.24	249.19	249.07 (94.07)	4.3
BP9	$C_{13}H_{14}O_3$	218.24	218.21	217.08 (57.80)	4.0
BP10	$C_{12}H_{14}O_3$	206.21	206.24	205.08 (66.7)	3.9
BP11	$C_9H_{10}NO_4$	196.11	196.18	195.9 (77.8)	3.2
BP12	$C_9H_7O_2$	147.11	147.15	146.9 (14.2)	2.5
BP13	$C_9H_{10}O_3$	166.06	166.14	165.01 (82.7)	2.8
BP14	$C_6H_4NO_2$	122.10	123.09	121.02 (52.3)	1.9

BP = by-product.

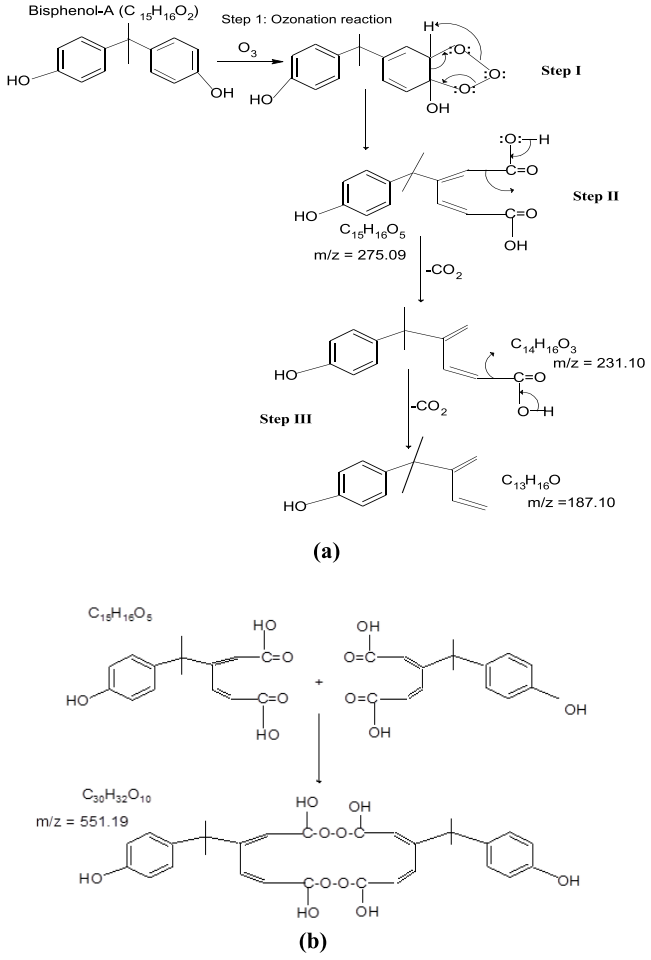

Figure 20. Proposed degradation pathways for the formation of BP1–BP4 from BPA using DBD alone. (a) Steps I to III, (b) step IV.

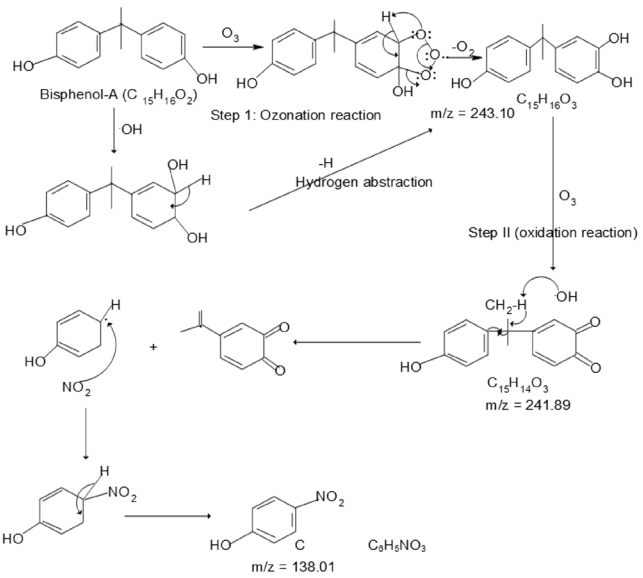

Figure 21. Proposed degradation pathways for the formation of BP5–BP7 from BPA using DBD alone and combined DBD/JT14 or DBD/photo-Fenton induced process.

photodegradation and combined TiO_2/UV/O_3 treatment of BPA are reported in the same vein in [7, 33]. The two authors established that BPA undergoes a hydroxylation reaction to produce the monohydroxylated compound ($C_{15}H_{16}O_3$). A similar molecular formula for BP6 during ozonation process of BPA is also reported in [34]. The oxidation of BP6 (which is removal of hydrogen) by either hydroxyl radicals or ozone produced BP7 ($C_{15}H_{14}O_3$). The attack by hydroxyl radicals on the methyl group (CH_3) in between the two aromatic rings resulted in hydrogen abstraction and C–C bond cleavage, which later produced the phenolic moiety and other residual intermediate compounds. Subsequently, the attack by the nitrogen oxides (NO_2 or NO) produced by DBD on the phenolic moiety, formed 4-nitrophenol as illustrated in figure 21.

3.10.3. Formation of BP8–BP10. In addition, the degradation routes of BPA leading to the formation of BP8–BP10 are illustrated in figure 22. The step by step attack of BPA molecules by hydroxyl radicals produced mono-, bi- and polyhydroxylated BPA. The polyhydroxylated BPA undergoes

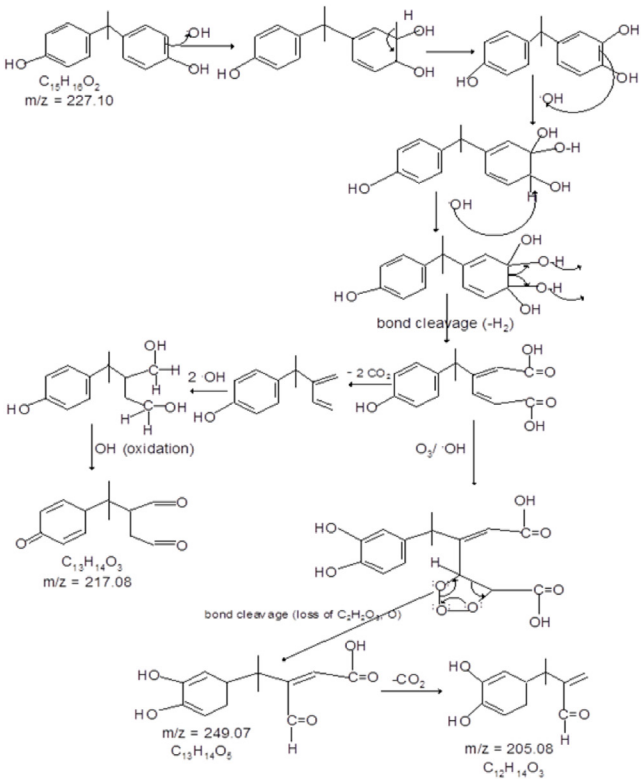

Figure 22. Proposed degradation pathways for the formation of BP8–BP10 from BPA using combined DBD with either supported catalyst or photo-Fenton induced reaction.

intramolecular rearrangement leading to C–C bond cleavage, loss of H_2 molecules thus forming BP1 ($C_{15}H_{16}O_5$).

More so, oxidation of BP1 in the presence of O_3/OH radicals or perhaps H_2O_2 in solution produced BP8 with molecular formula ($C_{13}H_{14}O_5$). This reaction was accompanied with loss of $C_2H_2O_3$ and atomic oxygen (O). Two consecutive CO_2 eliminations from BP1 and further oxidation in the presence of O_3/OH^0 yields compound BP9 ($C_{13}H_{14}O_3$). According to [34] compound BP9 was categorised as 3-formylacrylic acid derivative. While BP10 ($C_{12}H_{14}O_3$) was obtained from BP8 via CO_2 elimination as illustrated in figure 22.

3.10.4. Formation of BP11–BP14. The formation of BP11–BP14 starting with BP6 is presented in figure 23. As shown in figure 23, the initial hydroxylation of BP6 by hydroxyl radicals or direct attack by OH on the methyl group (CH_3) in between the two aromatic rings, resulted in hydrogen abstraction and subsequently ring cleavage leading to formation of smaller fragments (4-isopropenylcatechol and phenolic ion). The substitution on 4-isopropenylcatechol by one of the nitrogenous species (NO_2) yielded compound BP11 with molecular formula ($C_9H_{11}NO_4$). Likewise, the substitution of nitrous oxide (NO) on the phenolic ion liberated compound BP14 with chemical structure $C_6H_4NO_2$ (4-nitrosophenolate). The presence of nitrogenous oxide as part of the oxidation-products was a result of dry air used to generate ozone in the DBD system as nitrogen is a component of air. Also, oxidation of 4-isopropenylcatechol involving loss of hydrogen in the presence of O_3/OH^0/H_2O_2 produced compound BP12 ($C_9H_8O_2$).

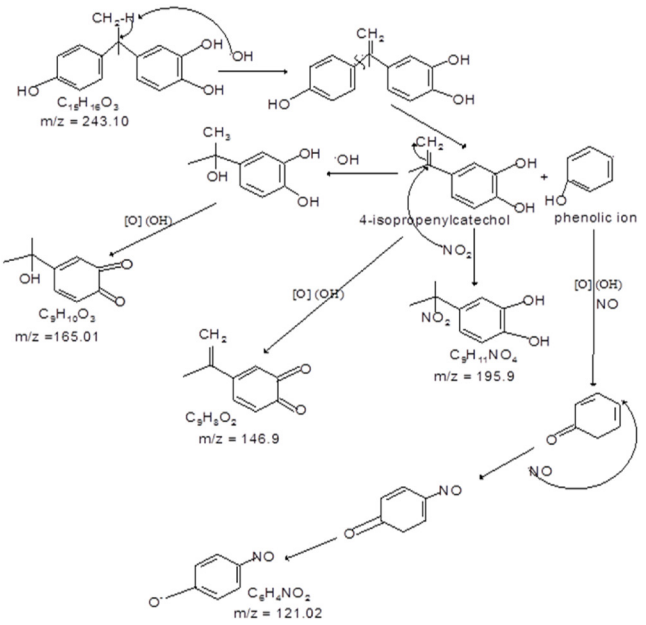

Figure 23. Proposed degradation pathways for the formation of BP11–BP14 from BPA using combined DBD with either supported catalyst or photo-Fenton induced reaction.

Further hydroxylation of BP12 by hydroxyl on the methylene group (CH_2) formed compound BP13 with molecular formula $C_9H_{10}O_3$. Fourteen major transformation products including oligomeric compounds were identified during BPA oxidation by single and combined AOTs. The following intermediates: BP1–BP4, BP6–BP7 have been extensively reported in the literature [6, 7, 33, 34]. While BP5, BP8, BP9–BP14 have not been reported in the literature. The differences in the intermediates proposed in this study compared to other studies may be attributed to the applied oxidation process and perhaps the types of free reactive species produced by the DBD system. The DBD produced O_3, H_2O_2, OH^0, where air containing nitrogen was used as a source of ozone generation. The ozonation process alone were used to study in [6, 34], combined TiO_2/UV/O_3 in [33], while powder commercial TiO_2 with UV to decompose BPA was utilized in [7]. It is clear from the previous studies that different advanced oxidation processes produce different free radicals and definitely result in different intermediate compounds. Critical analysis of the intermediates showed that BPA decomposed via ozonation step in the DBD while most intermediates in the combined system were proposed via hydroxylation and nitration steps respectively. In all, the degradation of BPA followed different steps: ozonation, hydroxylation, decarboxylation, and dimerization, double decarboxylation and nitration reaction. It is important to mention that unlike DBD alone, no dimeric or high molecular weight compounds were formed as intermediates in the two combined systems. This is in accordance with the results reported by [11] where there was no formation of oligomeric compounds during the degradation of phenol by combined pulsed plasma discharge and TiO_2 photocatalyst. Additionally, the most of the intermediates obtained with the combined system were of lower molecular mass compared to high molecular weight intermediates obtained with DBD alone. This

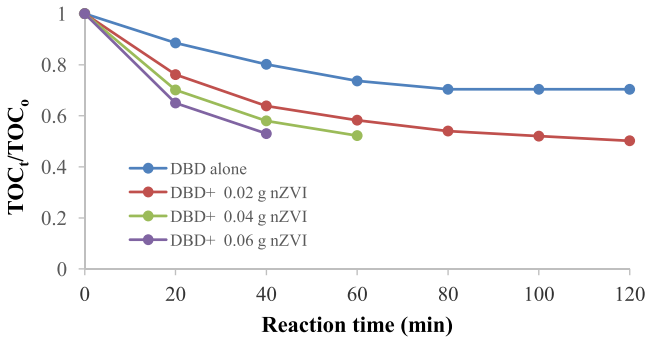

Figure 24. Mineralization of BPA by DBD and DBD/photo-Fenton induced process: solution pH 3, discharge voltage 8 kV, concentration of BPA 10 ppm, solution volume 1.5 L, number of replicates = 2.

further demonstrated that the incorporation of polyethylene glycol stabilized nano zero valent iron with DBD enhanced the mineralization of BPA much more than with DBD alone. Complete mineralization of BPA into CO_2 and H_2O was not achieved via the two approaches, which may be attributed to the DBD reactor type.

3.11. Mineralization of BPA

In order to compare the effectiveness of DBD alone and DBD/photo-Fenton induced process (JT17) for the degradation BPA, the mineralization rate was measured in terms of TOC. The TOC removal efficiency was evaluated using equation (7)

$$\text{TOC removal}(\%) = \frac{\text{TOC}_0 - \text{TOC}_t}{\text{TOC}_0} \times 100, \qquad (7)$$

where TOC_0 represents the initial value of TOC before exposure to DBD and DBD/photo-Fenton induced process,while TOC_t is final value of TOC after treatment.

The results of TOC removal of BPA by DBD or DBD/photo-Fenton induced process is presented in figure 24.

As shown in figure 24, the TOC removal rate of BPA increased with an increasing dosage of nZVI. For the DBD containing 0.02, 0.04 and 0.06 g nZVI, the TOC removal rate of BPA were 37.2%, 41.9% and 47.5% as compared to 20% by the DBD alone after 40 min. The argument put forward for such increment upon the addition of nZVI has been discussed earlier. The TOC removal rate of BPA upon addition of 0.06 g nZVI was 47.5% at 40 min. This demonstrated a slower mineralization rate when compared to 100% removal rate of BPA achieved within 40 min using DBD with 0.06 g nZVI. The possible explanation for the slower mineralization rate may be due to formation of persistent and stable intermediates which resisted further degradation. Nevertheless, the combined system significantly increased TOC removal rate compared to the DBD alone, as was also evident in the number of intermediates generated via each treatment process. The lower TOC removal rate by the DBD correlated well with the number of intermediate compounds generated. The TOC values found for the combined DBD with different dosages of nZVI may due to the existence of synergistic effects between the combined systems. The TOC value of 47.5% or 43.1% in this study was greater than 33% TOC removal rate reported by [22] during oxidation of sulfadiazine by DBD reactor containing powder ferrous ion. The improvement in the TOC removal rate in this study over the outcome reported by [22, 35] may be due to the small size, high surface area, and enhanced reactivity of nZVI compared to ferrous ion.

4. Conclusion

The chemistry of the degradation of aqueous solution of BPA in a radical environment using DBD alone and combined DBD with nano zero valent iron particles stabilised with polyethylene glycol including the operating parameters that influences the performance of the system have been fully established. The removal efficiency of BPA was mostly favoured in acidic conditions and at lower concentrations. Maximum BPA removal efficiency occurred at low pH (3) at an optimum concentration of 10 mg l^{-1}. The BPA degradation yield at 30 mg l^{-1} concentration of BPA after 80 min treatment time was 3.73×10^{-4} g kW^{-1} h^{-1}. It was shown that addition of 0.06 g nZVI to DBD plasma technology induced photo-Fenton like reaction gave 100% removal within 30 min and enhanced removal efficiency of BPA in aqueous solution which indicated the existence of synergetic effects. The TOC reduction value by the combined systems was however rather products low due to formation of recalcitrant transformation products. The degradation of BPA proceeded via ozonation, hydroxylation, dimerization, as well as decarboxylation and nitration steps were proposed. Five new oxidation products such as (BP5, BP11–BP14) of BPA which have not been previously reported in the literature were identified. This novel combined advanced technology has great potential for environmental remediation in the area of wastewater purification.

Acknowledgment

The authors acknowledge Water Research Commission, South Africa (Project number WRC/2013/K5/2364) for funding and the research and Environmental and Nano Sciences Group, Department of Chemistry, University of the Western Cape, South Africa for assistance with analysis and characterisation.

References

[1] Kolle S N, Ranmirez T, Kamp H G, Buesen R, Flick B and Strauss V 2013 *Regul. Toxicol. Pharm.* **63** 259
[2] Geens T, Goeyens L and Covaci A 2011 *Int. J. Hyg. Environ. Health* **214** 339
[3] Rogers J A, Metz L and Wee Yong V 2013 *Mol. Immunol.* **53** 421
[4] Jiang X, Wu Y, Wang P, Li H and Dong W 2013 *Environ. Sci. Pollut. Res.* **20** 4947
[5] Chen T C, Shue M F, Yeh Y L and Kao T J 2010 *Environ. Monit. Assess.* **161** 135
[6] Tay K S, Abd Rahman N and Radzi Bin Abas M 2012 *Maejo Int. J. Sci. Technol.* **6** 77

[7] Cardoso da Silva J C, Reis Teodoro J A, Franco Afonso R J C, Aquino S F and Augusti R 2014 *Rapid Commun. Mass Spectrom.* **28** 987
[8] Demierre A L, Peter R, Oberli A and Bourqui-Pittet M 2012 *Toxicol. Lett.* **213** 305
[9] Fan Z, Hu J, An W and Yan M 2013 *Environ. Sci. Technol.* **47** 10841
[10] Michałowicz J 2014 *Environ. Toxicol. Pharm.* **37** 738
[11] Wang Y, Sun H, Duan X, Ang H M, Tadé M O and Wang S 2015 *Appl. Catal.* B **172** 73
[12] Xu J, Wang L and Zhu Y 2012 *Langmuir* **28** 8418
[13] Tijani J O, Fatoba O O, Madzivire G and Petrik L F 2014 *Water Air Soil Pollut.* **225** 2102
[14] Jiang B, Qiu J Z S, Mingbo W, Yan Q Z Z and Xue Q 2014 *Chem. Eng. J.* **236** 348
[15] Locke B R, Sato M, Sunka P, Hoffmann M R and Chang J S 2006 *Ind. Eng. Chem. Res.* **45** 882
[16] Malik M A 2010 *Plasma Chem. Plasma Process.* **30** 21
[17] Magureanu M, Piroi D, Mandache N B, David V, Medvedovici A and Parvulescu V I 2010 *Water Res.* **44** 3445
[18] Magureanu M, Piroi D, Mandache N B, David V, Medvedovici A, Parvulescu V I and Bradu C 2011 *Water Res.* **45** 3407
[19] Gao L, Sun L, Wan S, Yu Z and Li M 2013 *Chem. Eng. J.* **228** 790
[20] Shahwan T, Abu Sirriah S, Nairat M, Boyaci E, Eroglu A E, Scott T B and Hallam K R 2011 *Chem. Eng. J.* **172** 258
[21] Liu Y, Mei S, Iya-Sou D, Cavadias S and Ognier S 2012 *Chem. Eng. Process.* **56** 10
[22] Rong S P, Sun Y B and Zhao Z H 2014 *Chin. Chem. Lett.* **25** 187
[23] Rong S and Sun Y 2013 *J. Chem. Technol. Biotechnol.* **89** 1351
[24] Dobrin D, Bradu C, Magureanu M, Mandache N B and Parvulescu V I 2013 *Chem. Eng. J.* **234** 389
[25] Lesage O, Falk L, Tatoulian M, Mantovani D and Ognier S 2013 *Chem. Eng. Process.* **72** 82
[26] Manoj Kumar Reddy P, Rama Raju B, Karuppiah J, Linga Reddy E and Subrahmanyam C 2013 *Chem. Eng. J.* **217** 41
[27] Hu J, Wang J and Chen R 2006 *Sci. China* B **49** 186
[28] Xi Y, Mallavarapu M and Naidu R 2010 *Mater. Res. Bull.* **45** 1361
[29] Li S, Ma X, Jiang Y and Cao X 2014 *Ecotoxicol. Environ. Safety* **106** 146
[30] Oputu O, Chowdhury M, Nyamayaro K, Fatoki O and Fester V 2015 *J. Environ. Sci.* **35** 83
[31] Goi A and Trapido M 2002 *Chemosphere* **46** 913
[32] Trapido M, Epold I, Bolobajev J and Dulova N 2014 *Environ. Sci. Pollut. Res.* **21** 12217
[33] Colombo A, Cappelletti G, Ardizzone S, Biraghi I, Bianchi C L, Meron D, Pirola C and Spadavecchia F 2012 *Environ. Chem. Lett.* **10** 55
[34] Deborde M, Rabouana S, Mazelliera P, Duguet J P and Legube B 2008 *Water Res.* **42** 4299
[35] Lee J, Park H and Yoon J 2003 *Environ. Technol.* **24** 241